

Estimating Hormone Concentrations in the Pituitary-Thyroid Feedback Loop from Irregularly Sampled Measurements*

Seth Siriya * Tobias M. Wolff * Isabelle Krauss *
Victor G. Lopez * Matthias A. Müller *

* Leibniz University Hannover, Institute of Automatic Control,
Germany, (e-mail: siriya, wolff, krauss, lopez, mueller@irt.uni-hannover.de).

Abstract: Model-based control techniques have recently been investigated for the recommendation of medication dosages to address thyroid diseases. These techniques often rely on knowledge of internal hormone concentrations that cannot be measured from blood samples. Moreover, the measurable concentrations are typically only obtainable at irregular sampling times. In this work, we empirically verify a notion of sample-based detectability that accounts for irregular sampling of the measurable concentrations on two pituitary-thyroid loop models representing patients with hypo- and hyperthyroidism, respectively, and include the internal concentrations as states. We then implement sample-based moving horizon estimation for the models, and test its performance on virtual patients across a range of sampling schemes. Our study shows robust stability of the estimator across all scenarios, and that more frequent sampling leads to less estimation error in the presence of model uncertainty and misreported dosages.

Keywords: Pituitary-thyroid feedback loop, hypothyroidism, hyperthyroidism, Hashimoto's thyroiditis, Graves' disease, irregular sampling, moving horizon estimation, detectability.

1. INTRODUCTION

The pituitary-thyroid (PT) feedback loop—illustrated in Fig. 1—is a key part of the endocrine system. Its functioning can be described as follows (Gardner and Greenspan, 2004). The pituitary gland secretes thyroid-stimulating hormone (TSH), stimulating the production of the hormones triiodothyronine (T_3) and thyroxine (T_4) by the thyroid gland, the latter of which is further converted into T_3 by 5'-deiodinase type I (D1) and 5'-deiodinase type II (D2) in the liver and kidneys. The production of TSH is then inhibited by T_4 via the pituitary, closing the loop, while thyrotropin-releasing hormone (TRH) produced by the hypothalamus stimulates TSH production.

Various diseases are associated with dysfunction of this loop. Hashimoto's thyroiditis is a disorder causing insufficient activity in the thyroid, leading to *hypothyroidism*. It is typically treated via the oral intake of levothyroxine (L- T_4) and sometimes levothyronine (L- T_3), which are synthetic replacements for T_4 and T_3 , respectively. In contrast, Graves' disease is a condition causing antibodies to overstimulate thyroid activity, leading to *hyperthyroidism*. It is often treated via the oral intake of antithyroid agents such as methimazole (MMI), inhibiting thyroid activity.

Historically, trial-and-error has been used to prescribe dosages based on measured T_4 , T_3 , and TSH concentrations from blood samples. This heuristic approach can take

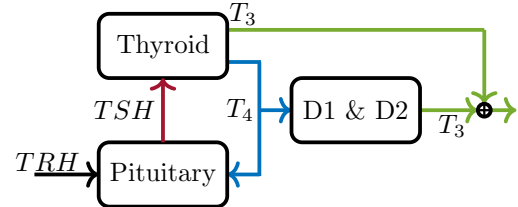


Fig. 1. Simple diagram of PT loop from Wolff et al. (2025).

a long time for restoration of normal thyroid function, during which patients may suffer from high dosages. Recently, systematic approaches have been investigated that combine models with algorithmic tools, including control-theoretic methods. In Yang et al. (2021), a model of the PT loop is proposed and analyzed. A model considering oral intake of L- T_4 is used to design pole-placement and model predictive control (MPC) schemes for dosage recommendation in Sharma et al. (2023, 2024). These works do not account for the influence of T_3 , which is known to be important for quality of life (Dietrich et al., 2012; Hoermann et al., 2017, 2015). On the other hand, Wolff et al. (2022a) extend a nonlinear model of the PT loop that accounts for T_3 from (Dietrich, 2002; Berberich et al., 2018) to consider oral intake of L- T_4 and L- T_3 , then apply nonlinear MPC for dosage recommendation. In the hyperthyroidism case, Theiler-Schwetz et al. (2022) combine a proportional-integral controller with a PT loop model to provide dosage recommendations for MMI, but neither T_3 nor oral intake of MMI are considered. In contrast, the nonlinear model in Wolff et al. (2025) considers these, and

* This project has received funding from the European Research Council (ERC) under the European Union's Horizon 2020 research and innovation programme (grant agreement No 948679).

is combined with MPC for dosage recommendation. However, the models from Wolff et al. (2022a, 2025) involve the internal concentrations of T_4 in the thyroid, alongside T_3 and TSH in the pituitary, as states, which *cannot* be readily measured from blood samples, motivating the use of state estimators. Although the peripheral T_4 , T_3 , and TSH concentrations *can* be measured from blood samples, testing can only occur irregularly.

To address the state estimation problem for nonlinear systems, the extended and unscented Kalman filter (Stengel, 1994; Julier and Uhlmann, 2004) are popular choices of observers due to their computational efficiency, but often produce inaccurate estimates for highly nonlinear models and unmodeled disturbances (Rawlings et al., 2022). Moving horizon estimation (MHE) overcomes these issues. It formulates the estimation task as an optimization problem over a finite horizon of past output measurements and inputs, given a known system model. Under a detectability notion known as incremental input/output-to-state stability (i-IOSS), robust stability of optimization-based observers such as MHE can be guaranteed (Allan and Rawlings, 2021; Ji et al., 2015; Knüfer and Müller, 2023; Schiller et al., 2023; Schiller and Müller, 2024). However, MHE requires constant, regular sampling of output measurements, which is not reasonable in the context of the PT loop, since blood samples are collected sparsely and irregularly. Recently, sample-based versions of i-IOSS and MHE that handle irregular measurements have been developed in Krauss et al. (2025b) and Krauss et al. (2025a), respectively.

Our contributions are as follows. Firstly, we formulate approximate discrete-time (DT) models of patients with hypo- and hyperthyroidism—based on Wolff et al. (2022a, 2025)—that are suitable for use by optimization-based observers, and empirically verify sample-based i-IOSS with respect to some outpatient and inpatient-relevant schemes for sampling peripheral T_4 , T_3 , and TSH. Secondly, we implement sample-based MHE for these DT systems. We test these algorithms on two virtual patients with hypo- and hyperthyroidism, and observe that our method is robustly stable across the sampling schemes, with performance improvements when sampling more frequently.

Notation Given $a, b \in \mathbb{Z}$, define $\mathbb{Z}_a := \mathbb{Z} \cap [a, \infty)$, and $\mathbb{Z}_a^b := \mathbb{Z} \cap [a, b]$. Given a set \mathcal{X} , \mathcal{X}^∞ denotes the set of all sequences $\{x_i\}_{i=0}^\infty$ satisfying $x_i \in \mathcal{X}$ for all $i \geq 0$. Given a vector $x \in \mathbb{R}^n$ and a matrix $P \succ 0$, $\|x\|_P = \sqrt{x^\top Px}$ denotes the weighted 2-norm. Given $t_2 > t_1 \geq 0$, a vector space \mathcal{S} , and a signal $s : [0, \infty) \rightarrow \mathcal{S}$, $s|_{[t_1, t_2]}(\tau) := s(t_1 + \tau)$ for $\tau \in [0, t_2 - t_1]$ is the truncation of s over $[t_1, t_2]$. The indicator function of a set A is denoted by $\mathbf{1}_A$.

2. SYSTEM MODELING

Continuous-time (CT) models of patients treated for hypo- and hyperthyroidism are provided in Sec. 2.1. In Sec. 2.2, we introduce the corresponding DT models used for MHE.

2.1 Continuous-time models

The CT model for hypothyroidism treatment is

$$\dot{x} = f_{\text{hypo}}(x, u, w). \quad (1)$$

The system state is $x = [T_{4,th} \ T_4 \ T_{3p} \ T_{3c} \ TSH \ TSH_c]^\top \in \mathbb{R}_{\geq 0}^6$, where T_4 (10^{-7} mol/l), T_{3p} (10^{-9} mol/l), and TSH (mIU/l) are the peripheral concentrations of T_4 , T_3 , and TSH, respectively, $T_{4,th}$ (10^{-12} mol/l) is the internal concentration of T_4 in the thyroid, and T_{3c} (10^{-8} mol/l), TSH_c (mIU/l), are the internal concentrations of T_3 , TSH, in the pituitary, respectively. Moreover, $u(t) = [u_{L-T_3}(t) \ u_{L-T_4}(t)]^\top \in \mathbb{R}_{\geq 0}^2$ is a known, time-varying input, where $u_{L-T_3}(t)$ and $u_{L-T_4}(t)$ describe the time-dependent absorption of the medications L-T₃ and L-T₄ (mol/l/s), and are computable given historical knowledge of L-T₃ and L-T₄ dosages taken by a patient via (A.8)–(A.9) in Appendix A. The evolution of the system is governed by f_{hypo} , which corresponds to the right-hand sides of equations (A.1)–(A.6). The model parameters are in Table C.1 within Appendix C, except $G_{T,co}$ —the scaling factor for the thyroid hormone production rate—is set to 0.1, representing an underactive thyroid. This model is obtained by modifying the original from Wolff et al. (2022a) to consider the process noise $w = [w_{G_{D1}} \ w_{G_{T3}} \ w_{TRH} \ w_{L-T_3} \ w_{L-T_4}]^\top \in \mathbb{R}^5$. We refer to that work for more details, and instead focus on describing our modifications. In particular, $w_{G_{D1}}$, $w_{G_{T3}}$, w_{TRH} , w_{L-T_3} , and w_{L-T_4} capture uncertainty in knowledge of the crucial parameters G_{D1} , G_{T3} , and TRH , alongside u_{L-T_3} and u_{L-T_4} due to misreported medication dosages. Compared to Wolff et al. (2022b), f_{hypo} is obtained by multiplying G_{D1} , G_{T3} , TRH , u_{L-T_4} , and u_{L-T_3} , with $(1 + w_{G_{D1}})$, $(1 + w_{G_{T3}})$, $(1 + w_{TRH})$, $(1 - w_{L-T_4})$, and $(1 - w_{L-T_3})$, respectively.

Next, we introduce an output model for the measured concentrations of peripheral T_4 , T_3 and TSH from blood samples: $y = h(x, v) := [(T_4 + v_{T_4}) \ (T_{3p} + v_{T_{3p}}) \ (TSH + v_{TSH})]^\top \in \mathbb{R}^3$, where $v = [v_{T_4} \ v_{T_{3p}} \ v_{TSH}]^\top \in \mathbb{R}^3$ is measurement noise.

The CT model for hyperthyroidism is

$$\dot{x} = f_{\text{hyper}}(x, u, w). \quad (2)$$

The state is $x \in \mathbb{R}_{\geq 0}^7$, which compared to hypothyroidism also includes \bar{MMI}_{th} , the concentration of MMI in the thyroid (10^{-5} mol/l). The known input is $u(t) = u_{MMI}(t) \in \mathbb{R}_{\geq 0}$, describing the absorption of MMI from the plasma to the thyroid (mol/l/s). Moreover, the process noise is $w = [w_{G_{D1}} \ w_{G_{T3}} \ w_{TRH} \ w_{MMI}]^\top \in \mathbb{R}^4$, where w_{MMI} captures uncertainty in u_{MMI} from misreported dosages. Development of f_{hyper} follows analogously to f_{hypo} , and is described in depth within Appendix B.

2.2 Approximate Discrete-Time Models

In this section, we describe the DT models based on Sec. 2.1 that will be used for sample-based MHE.

We start with the hypothyroidism case. Denote the solution to (2) at time t , initialized from a state $x \in \mathcal{X}_{\text{hypo}} \subseteq \mathbb{R}^6$ at time 0, and driven by a known signal $u : [0, t] \rightarrow \mathbb{R}_{\geq 0}$ and fixed process noise $w \in \mathcal{W}_{\text{hypo}} \subseteq \mathbb{R}^5$, by $\phi_{\text{hypo}}(t, x, u(\cdot), w)$. Let F_{hypo} be a discretized model of (1) satisfying $F_{\text{hypo}}(x, u(\cdot), w) \approx \phi_{\text{hypo}}(T_d, x, u(\cdot), w)$ for $x \in \mathcal{X}_{\text{hypo}}$, $w \in \mathcal{W}_{\text{hypo}}$, and $u(\cdot) \in \{\bar{U}_{[kT_d, (k+1)T_d]} \mid U(\cdot) \in$

$\mathbb{U}_{L-T}, k \in \mathbb{Z}_0\}$.¹ Here, T_d is the discretization period, which is chosen as $T_d = 8$ h in this work. Moreover, \mathbb{U}_{L-T} , is the set of possible u_{L-T_3} and u_{L-T_4} with up to 30 μg of L-T₃ and 400 μg of L-T₄ taken daily, as defined in (A.10) in Appendix A. This can be obtained via various numerical integration methods (e.g., Euler and Runge-Kutta), but we utilize the CVODES integrator in the SUNDIALS suite from Hindmarsh et al. (2005) due to the stiffness of (1).

We can then formulate the following DT system:

$$x_{k+1} = F_{\text{hypo}}(x_k, u_k(\cdot), w_k), \quad y_k = h(x_k, v_k),$$

with $x_k \in \mathcal{X}_{\text{hypo}}$, $y_k \in \mathcal{Y}_{\text{hypo}} \subseteq \mathbb{R}^3$, $w_k \in \mathcal{W}_{\text{hypo}}$, $v_k \in \mathcal{V} \subseteq \mathbb{R}^3$, and $u_k(\cdot) = U_{[kT_d, (k+1)T_d]}$ for $k \in \mathbb{Z}_0$, where $U(\cdot) \in \mathbb{U}_{L-T}$. Throughout, we consider $\mathcal{X}_{\text{hypo}} = [0.2, 0.6] \times [0.1, 1.4] \times [0.8, 3.1] \times [0.1, 1.3] \times [1.4, 6] \times [1.5, 6.3] (10^{-12} \text{ mol/l}, 10^{-7} \text{ mol/l}, 10^{-9} \text{ mol/l}, 10^{-8} \text{ mol/l}, \text{mIU/l}, \text{mIU/l})$, corresponding to low-to-normal thyroid activity, $\mathcal{W}_{\text{hypo}} = [-0.1, 0.1]^2 \times [-0.3, 0.3] \times \{0\} \times [0, 1]$,² $\mathcal{V} = [-0.1h(x_{\text{ss}}, 0), 0.1h(x_{\text{ss}}, 0)] (10^{-7} \text{ mol/l}, 10^{-9} \text{ mol/l}, \text{mIU/l})$, and $\mathcal{Y}_{\text{hypo}} = \mathcal{X}_{\text{hypo}} \oplus \mathcal{V}$, where $x_{\text{ss}} = [3.10 \ 1.17 \ 2.71 \ 1.12 \ 1.87 \ 1.99] (10^{-12} \text{ mol/l}, 10^{-7} \text{ mol/l}, 10^{-9} \text{ mol/l}, 10^{-8} \text{ mol/l}, \text{mIU/l}, \text{mIU/l})$ is the steady-state solution of (1) when $G_{T,\text{co}} = 1$ for a healthy individual. Denote $\mathbb{W}_{\text{hypo}} = \mathcal{W}_{\text{hypo}} \times \mathcal{V}$ for convenience.

Development of the hyperthyroidism DT system follows similarly, so we just describe the key differences. Denote the discretized dynamics by F_{hyper} . Analogously to hypothyroidism, we formulate the following DT system:

$$x_{k+1} = F_{\text{hyper}}(x_k, u_k(\cdot), w_k), \quad y_k = h(x_k, v_k),$$

with $x_k \in \mathcal{X}_{\text{hyper}} \subseteq \mathbb{R}^7$, $y_k \in \mathcal{Y}_{\text{hyper}} \subseteq \mathbb{R}^3$, $w_k \in \mathcal{W}_{\text{hyper}} \subseteq \mathbb{R}^4$, $v_k \in \mathcal{V} \subseteq \mathbb{R}^3$, and $u_k(\cdot) = U_{[kT_d, (k+1)T_d]}$ for $k \in \mathbb{Z}_0$, where $U(\cdot) \in \mathbb{U}_{MMI}$ and \mathbb{U}_{MMI} is the set of possible $u_{MMI}(\cdot)$ with up to 35 mg of MMI taken daily (defined in (B.4) in Appendix B). Throughout the paper, we will consider $\mathcal{X}_{\text{hyper}} = [0.2, 17] \times [0.4, 5] \times [1.2, 11] \times [0.4, 4.5] \times [0.6, 3.5] \times [0.7, 3.5] \times [0, 5] (10^{-12} \text{ mol/l}, 10^{-7} \text{ mol/l}, 10^{-9} \text{ mol/l}, 10^{-8} \text{ mol/l}, \text{mIU/l}, \text{mIU/l}, 10^{-5} \text{ mol/l})$, corresponding to normal–high thyroid activity, $\mathcal{W}_{\text{hyper}} = [-0.1, 0.1]^2 \times [-0.3, 0.3] \times [0, 1]$, and \mathcal{V} as before. Moreover, $\mathcal{Y}_{\text{hyper}} = \mathcal{X}_{\text{hyper}} \oplus \mathcal{V}$, and $\mathbb{W}_{\text{hyper}} = \mathcal{W}_{\text{hyper}} \times \mathcal{V}$ for convenience.

Throughout the paper, $(F, \mathcal{X}, \mathcal{Y}, \mathbb{U}, \mathbb{W})$ are placeholders, replaced by $(F_{\text{hypo}}, \mathcal{X}_{\text{hypo}}, \mathcal{Y}_{\text{hypo}}, \mathbb{U}_{L-T}, \mathbb{W}_{\text{hypo}})$ for hypothyroidism, or $(F_{\text{hyper}}, \mathcal{X}_{\text{hyper}}, \mathcal{Y}_{\text{hyper}}, \mathbb{U}_{MMI}, \mathbb{W}_{\text{hyper}})$ for hyperthyroidism.

3. VERIFYING DETECTABILITY

We first recall the definition of a sampling set and sample-based exponential i-IOSS from Krauss et al. (2025a).

Definition 1. (Sampling set). Consider a sampling interval sequence $\{\delta_i\}_{i=1}^{\infty}$ satisfying $\delta_i \in \mathbb{Z}_0$ for $i \in \mathbb{N}$ and

¹ We model $u(\cdot)$ as a CT signal since it can be symbolically expressed as a function of time via (A.8)–(A.9), which the CVODES integrator supports. However, w is fixed since it will be used as a decision variable when implementing MHE in Sec. 4.

² We consider $w_{L-T_3} \in \{0\}$ since we will only simulate a virtual patient medicated with L-T₄, which is consistent with treatment guidelines in Jonklaas et al. (2014). However, the general method is still applicable with $w_{L-T_3} \in [0, 1]$ for misreported L-T₃ dosages.

$\sup_i \delta_i < \infty$. Then, $K_i := \{\sum_{k=i}^{j+i-1} \delta_k \mid j \in \mathbb{N}\}$ is the associated infinite set of time instances from index i on, and $K := \{K_i \mid i \in \mathbb{N}\}$ is the corresponding sampling set.

Definition 2. (Sample-based exponential i-IOSS).

Consider a sampling set K . Then, the system (F, h) is sample-based exponentially i-IOSS with respect to K if there exist $\bar{P}_1, \bar{P}_2 \succ 0$, $\bar{Q}, \bar{R} \succeq 0$ and $\bar{\eta} \in [0, 1)$ such that for all $x_0, \tilde{x}_0 \in \mathcal{X}$, $\{\omega_i\}_{i=0}^{\infty}, \{\tilde{\omega}_i\}_{i=0}^{\infty} \in \mathbb{W}^{\infty}$, and $U(\cdot) \in \mathbb{U}$,

$$\begin{aligned} \|x_k - \tilde{x}_k\|_{\bar{P}_1}^2 &\leq \|x_0 - \tilde{x}_0\|_{\bar{P}_2}^2 \bar{\eta}^t + \sum_{j=0}^{k-1} \bar{\eta}^{k-j-1} \|\omega_j - \tilde{\omega}_j\|_{\bar{Q}}^2 \\ &\quad + \sum_{j \in \mathbb{Z}_0^{k-1} \cap K} \bar{\eta}^{k-j-1} \|y_j - \tilde{y}_j\|_{\bar{R}}^2 \end{aligned} \quad (3)$$

holds for all $k \geq 0$ and $K_i \in K$, where $\omega_k = [w_k^{\top} \ v_k^{\top}]^{\top}$, $\tilde{\omega}_k = [\tilde{w}_k^{\top} \ \tilde{v}_k^{\top}]^{\top}$, $u_k(\cdot) = U_{[kT_d, (k+1)T_d]}(\cdot)$, $\{(x_k, y_k)\}_{k=0}^{\infty}$ is the state-output trajectory associated with the initial state-input-noise triple $(x_0, \{u_k(\cdot)\}_{k=0}^{\infty}, \{\omega_k\}_{k=0}^{\infty})$, and $\{(\tilde{x}_k, \tilde{y}_k)\}_{k=0}^{\infty}$ is associated with $(\tilde{x}_0, \{u(\cdot)_k\}_{k=0}^{\infty}, \{\tilde{\omega}_k\}_{k=0}^{\infty})$.

Regular i-IOSS has become the standard detectability notion for nonlinear MHE in recent years (Allan and Rawlings, 2021; Schiller et al., 2023), but does not support irregular sampling. Instead, it was shown in Krauss et al. (2025a) that under the assumption of *sample-based* i-IOSS in Def. 2, robust global exponential stability can be established for the estimation error resulting from a sample-based version of MHE considering irregular sampling (described in Sec. 4). Thus, verification of sample-based i-IOSS is of interest, in order to evaluate suitability of the DT models from Sec. 2.2 for observer design with irregular measurements.

Table 1. Sequences of sampling intervals.

Notation	Defining rule	Interval description
$\{\delta_i^a\}_{i \in \mathbb{N}}$	$\delta_i^a = i$	8 hours
$\{\delta_i^b\}_{i \in \mathbb{N}}$	$\delta_i^b = \mathbb{1}_{[2, \infty)}(i) 3\delta_i^0$	1-1.5 weeks
$\{\delta_i^c\}_{i \in \mathbb{N}}$	$\delta_i^c = \mathbb{1}_{[2, \infty)}(i) (\delta_{2(i-1)}^b + \delta_{2(i-1)+1}^b)$	2-3 weeks
$\{\delta_i^d\}_{i \in \mathbb{N}}$	$\delta_i^d = \mathbb{1}_{[2, \infty)}(i) (\delta_{2(i-1)}^c + \delta_{2(i-1)+1}^c)$	4-6 weeks

$\{\delta_j^0\}_{j=1}^{\infty}$ is defined as $\delta_j^0 := 10 - |(j-2) \bmod 6 - 3|$ for $j \in \mathbb{N}$, producing the periodic sequence $\{8, 7, 8, 9, 10, 9, 8, 7, 8, \dots\}$.

To empirically verify sample-based i-IOSS for the hyperthyroidism model, we consider the sampling interval sequences from Table 1. Sequences $\{\delta_i^b\}_{i \in \mathbb{N}}$, $\{\delta_i^c\}_{i \in \mathbb{N}}$, $\{\delta_i^d\}_{i \in \mathbb{N}}$, correspond to outpatient settings with sparse, irregular sampling, and $\{\delta_i^a\}_{i \in \mathbb{N}}$ corresponds to an inpatient setting with frequent, regular sampling. We simulate 19800 trajectory pairs over 300 days, with initial states and noise sampled uniformly over $\mathcal{X}_{\text{hypo}}$ and \mathbb{W}_{hypo} , and known inputs from \mathbb{U}_{L-T} obtained by uniformly sampling the L-T₄ dosage each day over $[0, 40]$ μg . We denote K_i^l as the infinite set of time instances from interval $i \in \mathbb{N}$, and K^l as the sampling set, both generated by $\{\delta_i^l\}_{i=1}^{\infty}$ for $l \in \{a, b, c, d\}$. In the case of K^a , we empirically verify that (3) holds across all 19800 pairs over 300 days by choosing $\bar{P}_1 = I_6$, $\bar{P}_2 = 2 \cdot 10^3 I_6$, $\bar{\eta} = 0.95$, $\bar{Q} = 0.5 I_8$, and $\bar{R} = 0.5 I_3$. In the case of K^b , K^c , and K^d , (3) is satisfied by scaling \bar{R} to $5 \cdot 10^2 I_3$, $5 \cdot 10^3 I_3$, and $10^5 I_3$, respectively. For illustrative purposes, we plot the LHS and RHS of (3) for two random trajectory pairs in Fig. 2, for the set of time instances

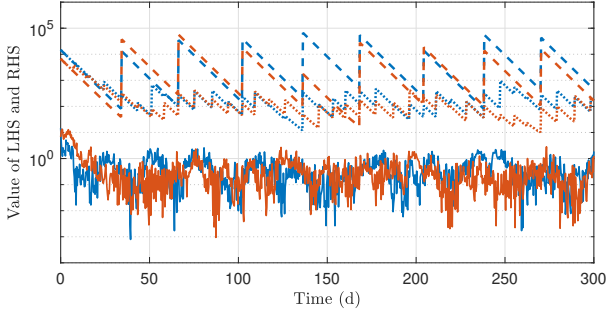


Fig. 2. LHS and RHS of (3) for two sampled trajectory pairs in the hypothyroidism scenario. The colors red and blue correspond to each pair. For each pair, the solid line corresponds to the LHS, and the dotted and dashed lines correspond to the RHS with sampled time instances in K_2^b and K_2^d , respectively.

K_2^b and K_2^d .³ The RHS typically decreases, but jumps at sampled time instances, such that the RHS remains higher than the LHS.

For hyperthyroidism, we empirically verify that (3) holds when choosing $\bar{P}_1 = I_7$, $\bar{P}_2 = 2 \cdot 10^3 I_7$, $\bar{\eta} = 0.96$, $\bar{Q} = 5I_7$, and $\bar{R} = 20I_3$ for K_2^a , and with \bar{R} increased to $3 \cdot 10^3 I_3$, $5 \cdot 10^4 I_3$, and $2 \cdot 10^6 I_3$, for K_2^b , K_2^c , and K_2^d , respectively.

4. SAMPLE-BASED MHE

In this section, we describe the sample-based MHE scheme used to estimate the unmeasured hormone concentrations at irregularly sampled time instances. It follows similarly to Krauss et al. (2025a), except we consider a *filtering* rather than a *prediction* form, so the state estimate at any given time considers the output measurement at that time (Rawlings et al., 2022, Ch. 4).⁴

Let $K_s \subseteq \mathbb{Z}_0$ be the set of time instances where a measurement is available to the estimator, and define the horizon length as $M_k := \min\{k, M\}$. At every time step $k \in K_s$ where a measurement is available, the following nonlinear program (NLP) is solved:

$$\begin{aligned} & \min_{\hat{x}_{k-M_k|k}, \hat{\omega}_{\cdot|k}} J(\hat{x}_{k-M_k|k}, \hat{\omega}_{\cdot|k}, \hat{y}_{\cdot|k}, k) \\ \text{s.t. } & \hat{x}_{j+1|k} = F(\hat{x}_{j|k}, u_j(\cdot), \hat{w}_{j|k}), \quad j \in \mathbb{Z}_{k-M_k}^{k-1}, \\ & \hat{y}_{j|k} = h(\hat{x}_{j|k}, \hat{v}_{j|k}), \quad j \in \mathbb{Z}_{k-M_k}^k, \\ & \hat{w}_{j|k} \in \mathcal{W}, \quad \hat{y}_{j|k} \in \mathcal{Y}, \quad j \in \mathbb{Z}_{k-M_k}^k, \\ & \hat{x}_{j|k} \in \mathcal{X}, \quad j \in \mathbb{Z}_{k-M_k}^k, \end{aligned}$$

where $u_j(\cdot) \in \mathbb{U}$. Here, $\hat{x}_{j|k}$ denotes the estimated state for time j computed at the current time k , and $\hat{\omega}_{j|k} = [\hat{w}_{j|k}^\top \hat{v}_{j|k}^\top]^\top$ and $\hat{y}_{j|k} \in \mathcal{Y}$ denote the estimated noise and outputs analogously. The optimal state sequence that solves the NLP at time k is denoted by $\hat{x}_{\cdot|k}^*$, and the

³ We illustrate K_2^l , $l \in \{b, d\}$, rather than the apparent choice K_1^l since $K_2^l \subseteq K_1^l$, and therefore if (3) holds for K_2^l , it holds for K_1^l . However, the trend in Fig. 2 is consistent across all K_i^l , $i \in \mathbb{N}$.

⁴ In practice, the time at which the value of measurements become known can vary widely depending on a range of factors, including whether inpatient or outpatient care is being exercised. We consider instantaneously known measurements for simplicity, and leave considering variation in the known time to future work.

optimal estimate at time k is given by $\hat{x}_k := \hat{x}_{k|k}^*$. We consider the following cost function:

$$J(\hat{x}_{k-M_k|k}, \hat{\omega}_{\cdot|k}, \hat{y}_{\cdot|k}, k) = 2\eta^{M_k} \|\hat{x}_{k-M_k|k} - \tilde{x}_{k-M_k}\|_P^2 + \sum_{j=k-M_k}^k \eta^{k-j} 2\|\hat{\omega}_{j|k}\|_Q^2 + \sum_{j \in \mathbb{Z}_{k-M_k}^k \cap K_s} \eta^{k-j} \|\hat{y}_{j|k} - y_j\|_R^2.$$

Here, \tilde{x}_k is the prior for the state used when solving the NLP, and is defined as $\tilde{x}_k := \hat{x}_k$ if $k > 0$, and $\tilde{x}_k := \chi$ if $k = 0$, where $\chi \in \mathcal{X}$ is the chosen prior at time $k = 0$. Moreover, $P \succ 0$ is a matrix penalizing the difference between the estimated state at the beginning of the horizon and the prior, and $Q, R \succeq 0$ are matrices penalizing the magnitude of the estimated disturbance sequence, and the difference between estimated and measured outputs, respectively. Finally, $\eta \in [0, 1]$ is a discount factor that determines the influence of past disturbances and measurements on the cost function. In contrast to the above, when $k \notin K_s$, such that there is no new information available, the estimate is instead computed via open-loop prediction by setting $\hat{x}_k := F(\hat{x}_{k-1}, u_{k-1}(\cdot), 0)$ if $k > 0$, and $\hat{x}_0 := \chi$ if $k = 0$.

The sample-based MHE scheme is applied for both hypo- and hyperthyroidism, with the set of sampled time steps K_s chosen to be K_1^a , K_1^b , K_1^c , and K_1^d . Note that $K_1^d \subseteq K_1^c \subseteq K_1^b \subseteq K_1^a$. In theory, the parameters P, Q, R , and η , can be chosen based on the matrices found in Sec. 3 to guarantee robust stability of the estimator (Krauss et al., 2025a). However, we manually tune these parameters in this work, which is typically done to achieve good performance in practice. In particular, for hypothyroidism, we set $P = \text{diag}(1, 0.1, 1, 1, 1, 1)$, $Q = \text{diag}(10, 1, 1, 0, 1, 1000, 1000, 100)$, and $R = \text{diag}(500, 500, 100)$, with $\eta = 0.7$, and $M = 20$. For hyperthyroidism, we set $P = \text{diag}(100, 0.1, 1, 1, 1, 1, 100)$, $Q = \text{diag}(10, 1, 1, 10, 1000, 1000, 100)$, $R = \text{diag}(250, 250, 1000)$, $\eta = 0.8$, and $M = 20$.

5. SIMULATION RESULTS

We now implement the sample-based MHE scheme from Sec. 4 using CasADi (Andersson et al., 2019) on simulated patients affected by hypo- and hyperthyroidism in Sec. 5.1 and 5.2, respectively, with the sets of sampled time instances K_1^a , K_1^b , K_1^c , and K_1^d .⁵

5.1 Hypothyroidism

We consider a simulation scenario for hypothyroidism where the patient initially does not take any medication. Then, they follow a simple oral L-T₄ medication strategy based on the guidelines provided in Jonklaas et al. (2014) starting from day 34. In particular, if the concentration of measured TSH is above the target range of 0.5–4 mIU/l on day 34, the patient initially takes a dosage of 136 µg/day (corresponding to an 80 kg human). Dose adjustments of 18.75 µg/day are then made up/down every 4–6 weeks, depending on whether measured TSH is above or below the target range, until it is reached. The corresponding signal $U(\cdot) \in \mathbb{U}_{L-T}$ is used when solving the MHE problem. However, we suppose the virtual patient

⁵ All code is available at <https://doi.org/10.25835/ly17bocm>.

forgets to take medication on days 39–43 and 81–85, which is not accounted for in the MHE scheme (i.e., $U(\cdot)$ does not reflect this), resulting in misreported dosages.

We simulated this scenario utilizing the model from (1), taking $U(\cdot)$ as the known input. However, we set $w_{L-T_4}(t) = 1 - U_{\text{true}}(t)/U(t)$ if $U(t) > 0$ and $w_{L-T_4}(t) = 0$ if $U(t) = 0$, to represent the misreported dosages, where $U_{\text{true}}(\cdot) \in \mathbb{U}_{L-T}$ denotes what the input would be if forgotten days are explicitly accounted for.⁶ Moreover, we set $w_{L-T_3}(t) = 0$ since it is known that the patient does not take $L-T_3$, $w_{G_{D1}}(t) = w_{G_{T3}}(t) = 0.1$ representing a patient with increased values for the parameters G_{D1} and G_{T3} , and $w_{TRH}(t) = 0.3 \cos(\pi(\frac{t}{43200} - \frac{5}{12}))$, capturing the circadian rhythm of TRH. Measurements are simulated by corrupting the value of T_4 , T_{3p} , and TSH , by a noise sampled from a uniform distribution over the set \mathcal{V} . We also set the initial state to $x(0) = [0.49 \ 0.18 \ 0.92 \ 0.18 \ 5.14 \ 5.48]^\top$, corresponding to the steady-state hormone concentrations for the virtual patient, and set the prior as $\chi = [0.2 \ 1.5 \ 3 \ 1.5 \ 2 \ 2]^\top$, where the units of both are $(10^{-12} \text{ mol/l}, 10^{-7} \text{ mol/l}, 10^{-9} \text{ mol/l}, 10^{-8} \text{ mol/l}, \text{mIU/l}, \text{mIU/l})$.

Plots of the true versus estimated states are shown in Figs. 3 and 4, with the former focusing on the measured concentrations T_4 , T_{3p} , and TSH , and the latter on the unmeasured concentrations $T_{4,th}$, T_{3c} , and TSH_c . Until day 34, all hormone concentrations oscillate around consistent values, due to the influence of $w_{TRH}(t)$. However, after day 34, T_4 , T_{3p} , and T_{3c} all increase, and TSH , $T_{4,th}$, and TSH_c , all decrease, except for days with forgotten dosages, where this trend is temporarily reversed. Despite the poor choice of prior χ , Fig. 4 shows that the estimates obtained via open-loop prediction after the first time step (8 h) are near the true states. This is because T_4 , T_{3p} and TSH are measured at $t = 0$ h, and the dynamics of $T_{4,th}$, T_{3c} and TSH_c have fast transient behavior. Moreover, the estimates are robustly stable for all sampling schemes, i.e., converge to a neighborhood of the true states. Interestingly, Fig. 3 shows that when sampling based on K_1^a , K_1^b and K_1^d , the estimates diverge from the true state after measurements.⁷ This is because the virtual patient is simulated with fixed noise (parameter uncertainty) $w_{G_{D1}}(t) = w_{G_{T3}}(t) = 0.1$, but for open-loop prediction between sampled time instances we set $w(t) = 0$, causing convergence of the estimates towards a different steady-state trajectory.

We also plot the sum of absolute errors (SAE) over all states as a function of time—defined as $\text{SAE}(k) = \sum_{i=0}^k \|\hat{x}_i - x(T_d i)\|_1$ —in Fig. 5. Before the first forgotten dosages, K_1^b has the worst SAE due to poor measurements on day 7. However, notice that K_1^b samples during both forgotten dosages, and K_1^c samples during the second forgotten dosages, resulting in improved performance at these times, compared to K_1^d which does not sample during either. On the other hand, K_1^a samples at every time step, and therefore not only accounts for the effects of the forgotten dosages, but even picks up intraday oscillations caused by $w_{TRH}(t)$, which can be seen in the

⁶ This choice of w_{L-T_4} implies $U(t)(1 - w_{L-T_4}(t)) = U_{\text{true}}(t)$.

⁷ This is most clearly seen after day 34, but also occurs beforehand.

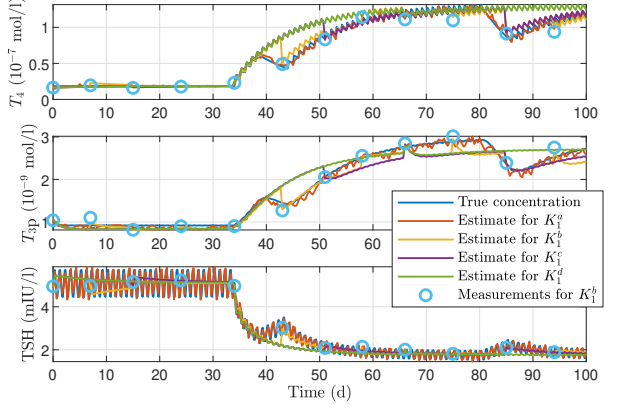


Fig. 3. Measured hormone concentrations of simulated patient with hypothyroidism, and their estimates, when sampling according to K_1^a , K_1^b , K_1^c , and K_1^d .

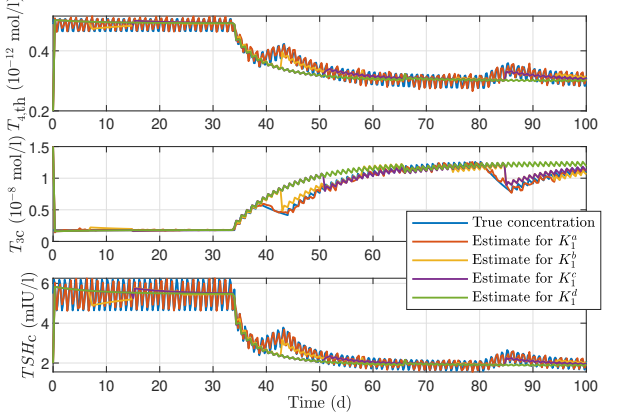


Fig. 4. Unmeasured hormone concentrations of simulated patient with hypothyroidism, and their estimates, when sampling according to K_1^a , K_1^b , K_1^c , and K_1^d .

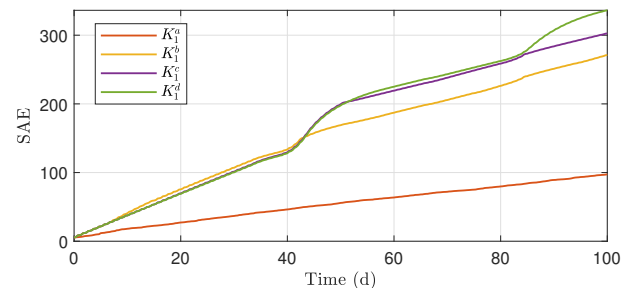


Fig. 5. SAE of estimates for simulated patients with hypothyroidism, when sampling according to K_1^a , K_1^b , K_1^c , and K_1^d .

TSH , $T_{4,th}$, and TSH_c plots across Figs. 3 and 4. These results make sense, since sampling frequently allows more information to be considered by the MHE algorithm to improve the estimates. They are further supported by the computed root mean square error (RMSE) values (defined as $\text{RMSE} = \sqrt{\frac{1}{T} \sum_{i=0}^T \|\hat{x}_i - x(T_d i)\|_2^2}$ where T is the number of simulated time steps), which were found to be 0.47 for K_1^a , 1.08 for K_1^b , 1.25 for K_1^c , and 1.34 for K_1^d .

5.2 Hyperthyroidism

Similar to Sec. 5.1, for the hyperthyroidism simulation, the patient initially does not take any medication, then follows a naive oral MMI medication strategy consistent with the rough guidelines from Ross et al. (2016). In particular, 7.5 mg/day is taken if the measured concentration of free T_4 (FT_4) is between 27–41 pmol/l, 15 mg/day is taken if FT_4 is within 41–54 pmol/l, and 35 mg/day is taken if FT_4 is above 54 pmol/l, with FT_4 computed from T_4 via (A.7) in Appendix A, and dosages updated when measurements are taken every 4–6 weeks. The corresponding signal $U(\cdot) \in \mathbb{U}_{L-T}$ is used when solving the MHE problem. The same forgotten dosages from Sec. 5.1 are considered, alongside the same sampling sequences from Table 1.

This scenario was simulated using the model from (2). Analogously to Sec. 5.1, $U(\cdot) \in \mathbb{U}_{MMI}$ is taken as the input, but we set $w_{MMI}(t) = 1 - U_{\text{true}}(t)/U(t)$ if $U(t) > 0$ and $w_{L-T_4}(t) = 0$ if $U(t) = 0$, where $U_{\text{true}}(\cdot) \in \mathbb{U}_{MMI}$ denotes the input if forgotten days are explicitly accounted for. Moreover, we also set $w_{G_{D1}}(t)$, $w_{G_{T3}}(t)$, and $w_{TRH}(t)$, to be the same as in Sec. 5.1. Measurements are simulated by corrupting the value of T_4 , T_{3p} , and TSH , by a noise sampled from a uniform distribution over the set \mathcal{V} . We also set the initial state as $[12.45 \ 4.68 \ 10.57 \ 4.28 \ 0.86 \ 0.92 \ 0]^\top$, and the MHE prior as $\chi = [7 \ 3 \ 7 \ 2 \ 2 \ 2.5 \ 1]^\top$, with the units (10^{-12} mol/l, 10^{-7} mol/l, 10^{-9} mol/l, 10^{-8} mol/l, mIU/l, mIU/l, 10^{-5} mol/l).

Plots of the true versus estimated unmeasured hormone concentrations are shown in Fig. 6. Until day 34, all concentrations steadily oscillate around consistent values, then afterwards, in general, $T_{4,\text{th}}$ and T_{3c} decrease, and TSH_c and MMI_{th} both increase, in response to the medication, except when dosages are forgotten. Qualitatively, the performance in this scenario is mostly consistent with Sec. 5.1, where the estimates are stable with respect to the true state, and improve with more frequent sampling. This can be observed in Fig. 6, and is also supported by the RMSE values, which were 3.03 for K_1^a , 5.52 for K_1^b , 6.07 for K_1^c , and 6.77 for K_1^d . The most noteworthy difference is that the estimation error is more significant during the misreported dosages for the hyperthyroidism case, compared to the hypothyroidism case. This can be explained by the increased complexity of the hyperthyroidism model, making state estimation more difficult.

6. CONCLUSION

In this work, we evaluated the suitability of PT loop models for state estimation with irregular measurements by verifying sample-based i-IOSS across various sets of sampled time instances, representing potential blood testing schedules across both inpatient and outpatient settings. We then implemented sample-based MHE schemes for these models, and tested them on virtual patients being medicated for hypo- and hyperthyroidism. While the estimation performance is robustly stable across all schemes, more frequent sampling decreases the estimation error in the presence of misreported forgotten dosages, even allowing behavior like oscillations operating at faster timescales to be tracked. For clinical practice, this suggests that a suitable sampling scheme should be chosen based on

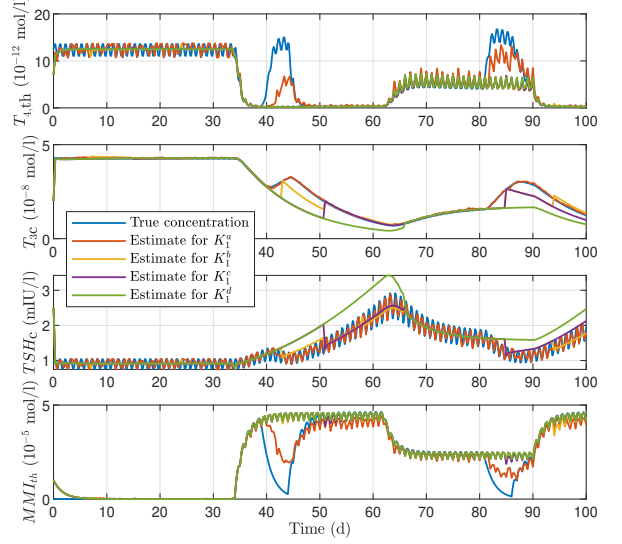


Fig. 6. Unmeasured hormone concentrations of simulated patient with hyperthyroidism, and their estimates, when sampling according to K_1^a , K_1^b , K_1^c , and K_1^d .

the certainty in the modeled dynamics and known input. If there is less certainty in this information (e.g., due to the risk of misreported dosages, such as in this study) then more frequent sampling is recommended to offset the effects of this. Moreover, sampling multiple times a day is required if accurate estimates throughout a day are important, which could be relevant in patients being monitored and treated for more severe forms of hyperthyroidism, such as thyrotoxicosis (Ross et al., 2016). In future work, we aim to combine the sample-based MHE schemes here with the MPC schemes from Wolff et al. (2022a) and Wolff et al. (2025). These previous works assume full state measurements, but the results from this paper can be used to make them applicable in realistic settings.

REFERENCES

Allan, D.A. and Rawlings, J.B. (2021). Robust stability of full information estimation. *SIAM Journal on Control and Optimization*, 59(5), 3472–3497.

Andersson, J.A., Gillis, J., Horn, G., Rawlings, J.B., and Diehl, M. (2019). Casadi: a software framework for nonlinear optimization and optimal control. *Mathematical Programming Computation*, 11(1), 1–36.

Berberich, J., Dietrich, J.W., Hoermann, R., and Müller, M.A. (2018). Mathematical modeling of the pituitary–thyroid feedback loop: role of a tsh-t3-shunt and sensitivity analysis. *Frontiers in endocrinology*, 9, 91.

Dietrich, J.W., Landgrafe, G., and Fotiadou, E.H. (2012). Tsh and thyrotropic agonists: key actors in thyroid homeostasis. *Journal of thyroid research*, 2012(1), 351864.

Dietrich, J.W.C. (2002). *Der Hypophysen-Schildrüsen-Regelkreis: Entwicklung und klinische Anwendung eines nichtlinearen Modells*. Logos-Verlag.

Gardner, D.G. and Greenspan, F.S. (2004). *Basic & Clinical Endocrinology*. McGraw-Hill, New York, 7th edition.

Hindmarsh, A.C., Brown, P.N., Grant, K.E., Lee, S.L., Serban, R., Shumaker, D.E., and Woodward, C.S. (2005). Sundials: Suite of nonlinear and differential/algebraic equation solvers. *ACM Transactions on Mathematical Software (TOMS)*, 31(3), 363–396.

Hoermann, R., Midgley, J.E., Dietrich, J.W., and Larisch, R. (2017). Dual control of pituitary thyroid stimulating hormone secretion by

thyroxine and triiodothyronine in athyreotic patients. *Therapeutic Advances in Endocrinology and Metabolism*, 8(6), 83–95.

Hoermann, R., Midgley, J.E., Larisch, R., and Dietrich, J.W. (2015). Homeostatic control of the thyroid–pituitary axis: perspectives for diagnosis and treatment. *Frontiers in endocrinology*, 6, 177.

Ji, L., Rawlings, J.B., Hu, W., Wynn, A., and Diehl, M. (2015). Robust stability of moving horizon estimation under bounded disturbances. *IEEE Transactions on Automatic Control*, 61(11), 3509–3514.

Jonklaas, J., Bianco, A.C., Bauer, A.J., Burman, K.D., Cappola, A.R., Celi, F.S., Cooper, D.S., Kim, B.W., Peeters, R.P., Rosenblath, M.S., et al. (2014). Guidelines for the treatment of hypothyroidism: prepared by the american thyroid association task force on thyroid hormone replacement. *Thyroid*, 24(12), 1670–1751.

Julier, S.J. and Uhlmann, J.K. (2004). Unscented filtering and nonlinear estimation. *Proceedings of the IEEE*, 92(3), 401–422.

Knüfer, S. and Müller, M.A. (2023). Nonlinear full information and moving horizon estimation: Robust global asymptotic stability. *Automatica*, 150, 110603.

Krauss, I., Lopez, V.G., and Müller, M.A. (2025a). Sample-based moving horizon estimation. *arXiv preprint arXiv:2510.24191*.

Krauss, I., Lopez, V.G., and Müller, M.A. (2025b). Sample-based nonlinear detectability for discrete-time systems. *IEEE Transactions on Automatic Control*, 70(4), 2422–2434. doi:10.1109/TAC.2024.3485486.

Rawlings, J.B., Mayne, D.Q., and Diehl, M.M. (2022). *Model Predictive Control: Theory, Computation and Design*. Nob Hill Publishing LLC, Santa Barbara, CA, USA, 2nd edition. 4th printing.

Ross, D.S., Burch, H.B., Cooper, D.S., Greenlee, M.C., Laurberg, P., Maia, A.L., Rivkees, S.A., Samuels, M., Sosa, J.A., Stan, M.N., et al. (2016). 2016 american thyroid association guidelines for diagnosis and management of hyperthyroidism and other causes of thyrotoxicosis. *Thyroid*, 26(10), 1343–1421.

Schiller, J.D. and Müller, M.A. (2024). Robust stability of moving horizon estimation for continuous-time systems. *at-Automatisierungstechnik*, 72(2), 120–133.

Schiller, J.D., Muntwiler, S., Köhler, J., Zeilinger, M.N., and Müller, M.A. (2023). A lyapunov function for robust stability of moving horizon estimation. *IEEE Transactions on Automatic Control*, 68(12), 7466–7481.

Sharma, R., Goede, S.L., Theiler-Schwetz, V., and Reichhartinger, M. (2024). Model predictive controller-based levothyroxine dosing strategy for patients suffering from hashimoto's thyroiditis. *IFAC-PapersOnLine*, 58(24), 275–280.

Sharma, R., Theiler-Schwetz, V., Trummer, C., Pilz, S., and Reichhartinger, M. (2023). Automatic levothyroxine dosing algorithm for patients suffering from hashimoto's thyroiditis. *Bioengineering*, 10(6), 724.

Stengel, R.F. (1994). *Optimal control and estimation*. Courier Corporation.

Theiler-Schwetz, V., Benninger, T., Trummer, C., Pilz, S., and Reichhartinger, M. (2022). Mathematical modeling of free thyroxine concentrations during methimazole treatment for graves' disease: development and validation of a computer-aided thyroid treatment method. *Frontiers in Endocrinology*, 13, 841888.

Wolff, T.M., Dietrich, J.W., and Müller, M.A. (2022a). Optimal hormone replacement therapy in hypothyroidism-a model predictive control approach. *Frontiers in endocrinology*, 13, 884018.

Wolff, T.M., Menzel, M., Dietrich, J.W., and Müller, M.A. (2025). Modeling and predictive control for the treatment of hyperthyroidism. *IFAC-PapersOnLine*, 59(1), 235–240.

Wolff, T.M., Veil, C., Dietrich, J.W., and Müller, M.A. (2022b). Mathematical modeling and simulation of thyroid homeostasis: Implications for the allan-herndon-dudley syndrome. *Frontiers in Endocrinology*, 13, 882788.

Yang, B., Tang, X., Haller, M.J., Schatz, D.A., and Rong, L. (2021). A unified mathematical model of thyroid hormone regulation and implication for personalized treatment of thyroid disorders. *Journal of Theoretical Biology*, 528, 110853.

Appendix A. PT LOOP MODEL FOR HYPOTHYROIDISM

The model f_{hypo} from (1) is defined such that the following system of equations is satisfied:

$$\begin{aligned} \frac{dT_{4,th}(t)}{dt} = & 10^{12} \alpha_{th} \left(G_{T,nom} G_{T,co} \frac{TSH(t)}{TSH(t) + D_T} \right. \\ & - G_{MCT8} \frac{T_{4,th}(t)}{10^{12} K_{MCT8} + T_{4,th}(t)} \\ & - G_{D1} (1 + w_{G_{D1}}) \frac{T_{4,th}(t) \frac{TSH(t)}{TSH(t) + k_{Dio}}}{T_{4,th}(t) \frac{TSH(t)}{TSH(t) + k_{Dio}} + 10^{12} K_{M1}} \\ & \left. - G_{D2} \frac{T_{4,th}(t) \frac{TSH(t)}{TSH(t) + k_{Dio}}}{T_{4,th}(t) \frac{TSH(t)}{TSH(t) + k_{Dio}} + 10^{12} K_{M2}} \right) - \beta_{th} T_{4,th}(t) \end{aligned} \quad (\text{A.1})$$

$$\begin{aligned} \frac{dT_4(t)}{dt} = & 10^7 \alpha_T \left(G_{MCT8} \frac{T_{4,th}(t)}{10^{12} K_{MCT8} + T_{4,th}(t)} \right. \\ & + u_{L-T_4}(t) (1 - w_{L-T_4}(t)) \left. \right) - \beta_T T_4(t) \end{aligned} \quad (\text{A.2})$$

$$\begin{aligned} \frac{dT_{3p}(t)}{dt} = & 10^9 \alpha_{31} (G_{D1} (1 + w_{G_{D1}}) \cdot \\ & \frac{T_{4,th}(t) \frac{TSH(t)}{TSH(t) + k_{Dio}}}{T_{4,th}(t) \frac{TSH(t)}{TSH(t) + k_{Dio}} + 10^{12} K_{M1}} + G_{D2} \frac{FT_4(t)}{FT_4(t) + K_{M2}} + \\ & G_{D2} \frac{T_{4,th}(t) \frac{TSH(t)}{TSH(t) + k_{Dio}}}{T_{4,th}(t) \frac{TSH(t)}{TSH(t) + k_{Dio}} + 10^{12} K_{M2}} + G_{D1} (1 + w_{G_{D1}}) \cdot \\ & \frac{FT_4(t)}{FT_4(t) + K_{M1}} + G_{T3} (1 + w_{G_{T3}}) \frac{TSH(t)}{D_t + TSH(t)} \end{aligned}$$

$$\begin{aligned} & + u_{L-T_3}(t) (1 - w_{L-T_3}(t)) \left. \right) - \beta_{31} T_{3p}(t) \end{aligned} \quad (\text{A.3})$$

$$\frac{dT_{3c}(t)}{dt} = 10^8 \alpha_{32} G_{D2} \frac{FT_4(t)}{FT_4(t) + K_{M2}} - \beta_{32} T_{3c}(t) \quad (\text{A.4})$$

$$\begin{aligned} \frac{dTSH(t)}{dt} = & \frac{\alpha_s G_H TRH (1 + w_{TRH})}{TRH (1 + w_{TRH}) + D_H} \\ & \cdot \frac{1}{(1 + S_s \frac{TSH_c(t)}{TSH_c(t) + D_s}) (1 + L_s G_R \frac{T_{3N}(t)}{T_{3N}(t) + D_R})} - \beta_S TSH(t) \end{aligned} \quad (\text{A.5})$$

$$\begin{aligned} \frac{dTSH_c(t)}{dt} = & \frac{\alpha_{S2} G_H TRH (1 + w_{TRH})}{(TRH (1 + w_{TRH}) + D_H) (1 + S_s \frac{TSH_c(t)}{TSH_c(t) + D_s})} \\ & \cdot \frac{1}{(1 + L_s G_R \frac{T_{3N}(t)}{T_{3N}(t) + D_R})} - \beta_{S2} TSH_c(t). \end{aligned} \quad (\text{A.6})$$

Here,

$$FT_4 = 10^{-7} T_4 / (1 + K_{41} TBG + K_{42} TBPA), \quad (\text{A.7})$$

$$FT_3 = 10^{-9} T_{3p} / (1 + K_{30} TBG), \text{ and}$$

$$T_{3N} = 10^{-8} T_{3c} / (1 + K_{31} IBS), \text{ all with the units mol/l.}$$

Let $\{t_i\}_{i=0}^{\infty}$ satisfying $t_i = 24 \cdot 3600 \cdot i$ represent the time instances where L-T₃ and L-T₄ is taken, in seconds, and let $\{m_{D3,i}\}_{i=0}^{\infty} \in [0, 30]^{\infty}$ and $\{m_{D4,i}\}_{i=0}^{\infty} \in [0, 400]^{\infty}$ be the corresponding dosages (in μg). Then, the time-dependent absorption of L-T₃ and L-T₄ are given by

$$u_{L-T3}(t) = k_{33} \frac{k_{13}}{k_{13} - (k_{23} + k_{33})} \sum_{i \in \mathbb{Z}_0} m_{D3,i} \mu(t - t_i) \cdot (e^{-(k_{23} + k_{33})(t - t_i)} - e^{-k_{13}(t - t_i)}), \quad (\text{A.8})$$

with the units mol/l/s, and

$$u_{L-T4}(t) = k_{34} \frac{k_{14}}{k_{14} - (k_{24} + k_{34})} \sum_{i \in \mathbb{Z}_0} m_{D4,i} \mu(t - t_i) \cdot (e^{-(k_{24} + k_{34})(t - t_i)} - e^{-k_{14}(t - t_i)}), \quad (\text{A.9})$$

in mol/l/s, for $t \geq 0$, where $\mu(t) := 0$ for $t < 0$ and $\mu(t) := 1$ for $t \geq 0$ is the Heaviside step function. Define

$$\mathbb{U}_{L-T} := \{[u_{L-T3}(\cdot) \ u_{L-T4}(\cdot)]^\top \mid (\text{A.8}), (\text{A.9}) \text{ satisfied for some } \{m_{D3,i}\}_{i=0}^\infty \in [0, 30]^\infty \text{ and } \{m_{D4,i}\}_{i=0}^\infty \in [0, 400]^\infty\}, \quad (\text{A.10})$$

representing the set of all possible u_{L-T_3} and u_{L-T_4} when up to 30 μg and 400 μg of L-T₃ and L-T₄ are taken daily.

Appendix B. PT LOOP MODEL FOR HYPERHYROIDISM

We describe the model of the PT loop for patients with hyperthyroidism undergoing treatment given by

$$\dot{x} = f_{\text{hyper}}(x, u, w),$$

in more detail compared to Sec. 2.1. The variable $x = [T_{4,th} \ T_4 \ T_{3p} \ T_{3c} \ TSH \ TSH_c \ MMI_{th}]^\top \in \mathbb{R}_{\geq 0}^7$, with the units (10^{-12} mol/l, 10^{-7} mol/l, 10^{-9} mol/l, 10^{-8} mol/l, mIU/l, mIU/l, 10^{-5} mol/l), is the system state, which, compared to Appendix A, includes MMI_{th} , the concentration of MMI in the thyroid. The system dynamics f_{hyper} corresponds to the right-hand side of equations (A.2)–(A.6), alongside (B.1) and (B.2), which are given as follows:

$$\begin{aligned} \frac{dT_{4,th}(t)}{dt} &= 10^{12} \alpha_{th} \left(G_T(t) \frac{TSH(t)}{TSH(t) + D_T} \right. \\ &\quad - G_{MCT8} \frac{T_{4,th}(t)}{10^{12} K_{MCT8} + T_{4,th}(t)} \\ &\quad - G_{D1} (1 + w_{G_{D1}}) \frac{T_{4,th}(t) \frac{TSH(t)}{TSH(t) + k_{Dio}}}{T_{4,th}(t) \frac{TSH(t)}{TSH(t) + k_{Dio}} + 10^{12} K_{M1}} \\ &\quad \left. - G_{D2} \frac{T_{4,th}(t) \frac{TSH(t)}{TSH(t) + k_{Dio}}}{T_{4,th}(t) \frac{TSH(t)}{TSH(t) + k_{Dio}} + 10^{12} K_{M2}} \right) \\ &\quad - \beta_{th} T_{4,th}(t), \end{aligned} \quad (\text{B.1})$$

where $G_T(t) = G_{T,nom} G_{T,co} TPO_a(t)$, $TPO_a(t) = c_0 (1 + \exp(-c_1(-10^{-5} MMI_{th}(t))^{1/c_2} + c_3)))^{-1}$, and

$$\frac{dMMI_{th}(t)}{dt} = 10^5 u_{MMI}(t) (1 - w_{MMI}(t)) - \beta_{M,th} MMI_{th}(t). \quad (\text{B.2})$$

The parameters are from Table C.1, except that we choose $G_{T,co} = 7$, representing an overactive thyroid. This model is obtained by modifying the one from Wolff et al. (2025) to consider process noise $w = [w_{G_{D1}} \ w_{G_{T3}} \ w_{TRH} \ w_{MMI}]^\top \in \mathbb{R}^4$. We refer to Wolff et al. (2025) for further details about the model, and focus on describing our modifications. The variables $w_{G_{D1}}$, $w_{G_{T3}}$, and w_{TRH} , are the same as the hypothyroidism case. However, w_{MMI} captures uncertainty in knowledge of u_{MMI} potentially caused by

misreported medication, such that compared to Wolff et al. (2025), (B.2) is obtained by multiplying u_{MMI} with $(1 - w_{MMI})$. The known, time-varying input is $u(t) = u_{MMI}(t) \in \mathbb{R}_{\geq 0}$, which describes the time-dependent absorption of MMI from the plasma to the thyroid (in mol/l/s). This can be computed given historical knowledge of the MMI dosages taken by the patient as follows:

$$u_{MMI}(t) = \alpha_{M,th} G_{M,th} \frac{MMI_{Pl}(t)}{K_{M,th} + MMI_{Pl}(t)}. \quad (\text{B.3})$$

Here, MMI_{Pl} denotes the concentration of MMI in the plasma. To define it, let $\{t_i\}_{i=0}^\infty$ satisfying $t_i = 24 \cdot 3600 \cdot i$ represent the time instances where MMI is orally taken, in seconds, and let $\{m_{MMI,i}\}_{i=0}^\infty \in [0, 35]^\infty$ be the corresponding dosages (in mg). Then, MMI_{Pl} is given by

$$MMI_{Pl}(t) = \frac{f_b k_a}{V(k_a - k_e)} \sum_{i \in \mathbb{Z}_0} m_{MMI,i} \mu(t - t_i) \cdot (e^{-k_e(t - t_i)} - e^{-k_a(t - t_i)}).$$

For convenience, we also define

$$\mathbb{U}_{MMI} := \{u_{MMI}(\cdot) \mid (\text{B.3}) \text{ is satisfied for some } \{m_{MMI,i}\}_{i=0}^\infty \in [0, 35]^\infty\}, \quad (\text{B.4})$$

representing the set of all possible $u_{MMI}(\cdot)$ when up to 35 mg of MMI is taken daily.

Appendix C. PARAMETERS

All model parameters are in Table C.1.

Table C.1. Fixed parameters across all models.

Parameter	Value	Parameter	Value
TBG	300 nmol/l	$TBPA$	4.5 $\mu\text{mol/l}$
IBS	8 $\mu\text{mol/l}$	TRH	6.9 nmol/s
G_H	817 mIU/s	D_H	47 nmol/s
α_S	0.4 l^{-1}	β_S	$2.3 \cdot 10^{-4} \text{ s}^{-1}$
L_S	1.68 $\text{l}/\mu\text{mol}$	$G_{T,nom}$	3.4 pmol/s
D_T	2.75 mIU/l	α_T	0.1 l^{-1}
β_T	$1.1 \cdot 10^{-6} \text{ s}^{-1}$	K_{M1}	500 nmol/l
α_{31}	$2.6 \cdot 10^{-2} \text{ l}^{-1}$	β_{31}	$8 \cdot 10^{-6} \text{ s}^{-1}$
G_{D2}	4.3 fmol/s	K_{M2}	1 nmol/l
α_{32}	$1.3 \cdot 10^{-5} \text{ l}^{-1}$	β_{32}	$8.3 \cdot 10^{-4} \text{ s}^{-1}$
α_{S2}	$2.6 \cdot 10^5 \text{ l}^{-1}$	β_{S2}	140 s $^{-1}$
D_R	100 pmol/l	G_R	1 mol/s
S_S	100 l/mIU	D_S	50 mIU/l
K_{30}	$2 \cdot 10^9 \text{ l}/\text{mol}$	K_{31}	$2 \cdot 10^9 \text{ l}/\text{mol}$
K_{41}	$2 \cdot 10^{10} \text{ l}/\text{mol}$	K_{42}	$2 \cdot 10^8 \text{ l}/\text{mol}$
α_{th}	250 l^{-1}	β_{th}	$4.4 \cdot 10^{-6} \text{ s}^{-1}$
k_{Dio}	1 mIU/l	K_{MCT8}	$4.7 \cdot 10^{-6} \text{ mol/l}$
G_{D1}	$1.98 \cdot 10^{-8} \text{ mol/s}$	G_{T3}	$23.1 \cdot 10^{-13} \text{ mol/s}$
G_{MCT8}	$1.94 \cdot 10^{-6} \text{ mol/s}$	c_0	0.97
$G_{M,th}$	$1.92 \cdot 10^{-12} \text{ mol/s}$	c_1	$1.47 \cdot 10^4$
$K_{M,th}$	$7.28 \cdot 10^{-7} \text{ mol/l}$	c_2	$1.36 \cdot 10^4$
$\alpha_{M,th}$	250 l^{-1}	c_3	$3.23 \cdot 10^4$
$\beta_{M,th}$	$6.42 \cdot 10^{-6} \text{ s}^{-1}$	f_b	0.93
k_a	1.02 l/h	k_e	0.106 l/h
V	281		